

Comparison of Silicon Carbide and Zircaloy4 Cladding during LBLOCA



Prepared By: Kwangwon Ahn

Prepared For: 22.314

Prepared On: December 7th, 2006

Comparison of Silicon Carbide and Zircaloy4 Cladding during LBLOCA

Kwangwon Ahn

Department of Nuclear Science and Engineering
Massachusetts Institute of Technology

Abstract

The pressure and temperature histories on cladding inner and outer surfaces during of LBLOCA (Large Break Loss of Coolant Accident) are considered as boundary conditions for the structural analyses of three cladding materials. Since SiC (Silicon Carbide) has higher yield and ultimate strengths than Zry-4 (Zircaloy-4) under the same primary stresses, SiC has higher primary safety margin than Zry-4. The temperature history, the large oscillation after the LBLOCA for all three cladding materials, is modeled the secondary stresses. But the secondary stresses converge as cladding outer pressure converges. All three cladding materials have sufficient safety margins in the secondary stress intensity.

1. Introduction

SiC is considered as one of the candidates for wall material of a fusion reactor, where a high-temperature and high-radiation environment is expected. Also, SiC showed its potential as a coating material for a high temperature gas-cooled reactor fuel. Thus, the resistance of SiC to the high-temperature and high-radiation environment can be a good reason for applying SiC as a cladding material for light water nuclear reactor. However, the brittle nature of SiC can be an important issue to be investigated. In addition, the degradation of SiC thermal conductivity after irradiation can also hurt its performance. Therefore, issues regarding SiC properties will be studied under PWR (Pressurized Water Reactor) LBLOCA situation.

This paper is organized as follows: First, the material properties of SiC and Zry-4 alloy are compared to each other. Second, the theoretical basis for structural analysis will be briefly introduced. Finally, the boundary conditions for the structural analysis will be presented. The boundary conditions, such as pressure and temperature histories, are obtained from RELAP5 modeling of typical Westinghouse PWR under LBLOCA transient. This will be followed by the calculation results of important stresses of SiC and Zry-4 cladding during LBLOCA, and their safety margins will be discussed. In conclusion, summary of the results and future work are suggested.

2. PWR Fuel Design

PWR fuel assembly is a bundle of cylindrical rods placed in a square lattice. The cylindrical rod is a tube filled with uranium oxide ceramic pellets. A gap between the pellets and the cladding tube is filled with helium gas to improve the conduction heat transfer from the fuel pellets to the cladding. There are 264 fuel rods per fuel assembly, and 193 fuel assemblies are loaded into a reactor core. The fuel rods are placed as 17×17 square lattice in an assembly. PWR fuel assemblies are about 4 meters tall. More specific design feature and parameters are shown in Figure 4-1 and Table 2-1.

Table 2-1 Fuel and Cladding Properties for Typical 4 Loop-PWR
(17x17 Square Rod Array)

Dimension	Unit	Value
Cladding Thickness	mm	0.57
Cladding Inside Diameter	mm	4.18
Gap Thickness	mm	0.121
Fuel Pellet Diameter	mm	8.19
Fuel Rod Diameter	mm	9.5
Active Fuel Height	m	3.66
U-235 Enrichment	wt %	2.6
Fuel Rod Pitch	mm	12.6
Channel Effective Flow Area	m ²	0.02458
Number of Rod Locations	number	289
Number of Fuel Rod	number	264

Two flow channels represent the whole core in the RELAP5 simulation: one (192 fuel assemblies) represents a core-average channel and the other (1 fuel assembly) simulates a hot channel, where a single hot rod is connected to the hot channel together with the hot assembly rods. Core bypass channel is modified to reflect the physical geometry.

The gap is initially filled with helium gas at pressure of 1.7MPa in typical PWR. The gap pressure will increase due to the fission gas release. However, the gap pressure is assumed as a constant, 8.32MPa, from steady state to LBLOCA considering the fission gas release. This is a conservative assumption since during LBLOCA higher gap pressure will exert higher stress in the cladding, when the core is fully depressurized.

3. Material Properties

Zry-4 and SiC are selected for the cladding materials in this study. Zry-4 is currently used as a cladding material in a light water reactor due to its small neutron capture cross section and mechanical stability. SiC is also a good material for maintaining its integrity at high temperature and in highly irradiated environment such as a fusion reactor. Several material properties are shown in Table 3-1 which is going to be utilized in the structural analyses of Zry-4 and SiC.

Table 3-1 Properties of Zry-4 and SiC

	Zry-4	SiC
Coefficient of Thermal Expansion	$6 \mu m / m^{\circ} K$	$3 \mu m / m^{\circ} K$
Modulus of Elasticity	$99.3 GPa$	$410 GPa$
Poisson's Ratio	0.37	0.21
Yield Strength	$170 MPa$	$450 MPa$
Ultimate Tensile Strength	$241 MPa$	$450 MPa$

Zry-4 properties are based on W. Chang^[7] and S. Tong^[10]. Coefficient of thermal expansion is taken at the range from 20°C to 800°C, which covers normal and accident condition of PWR. The yield strength and ultimate tensile strength are the values at 288°C, which is close to normal operating condition of PWR.

The thermal expansion coefficient of SiC is adopted from D. Carpenter's work^[2]. And the modulus of elasticity and Poisson's ratio are for *Direct Sintered Silicon Carbide* at 20°C, which are taken from CoorsTek^[8]. The ultimate tensile strength is also the value at 20°C from J. DiCarlo's work^[9]. Although the temperature is very different from the normal operating condition of PWR, these values do not vary too much with the temperature. Since brittle materials, such as SiC, experience little plastic deformation before fracture occurs, the yield strength of SiC is set to be equal to the ultimate tensile strength.

Figure 3-1 shows the thermal conductivities of SiC and Zry-4. In case of SiC, two cases are investigated: un-irradiated SiC (Case1) and irradiated SiC (Case2). This is because SiC can be easily irradiated and changed its thermal conductivity after burning the fuel. And Figure 3-2 shows the specific heat of Zry-4^[10] and SiC. These two figures are used as input data in RELAP5 model in order to capture the BC.

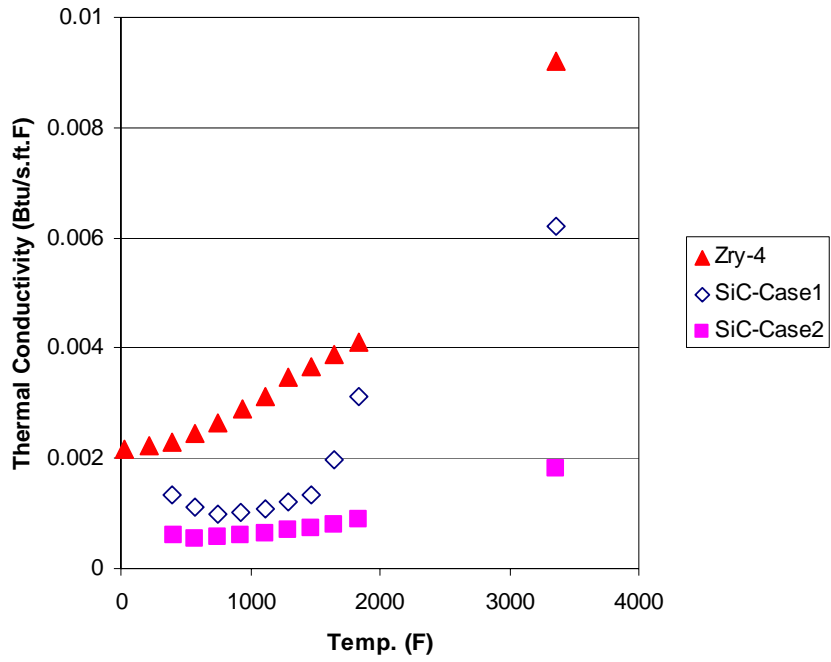


Figure 3-1 Thermal Conductivity of Zry-4 and SiC (Un-irradiated and Irradiated)

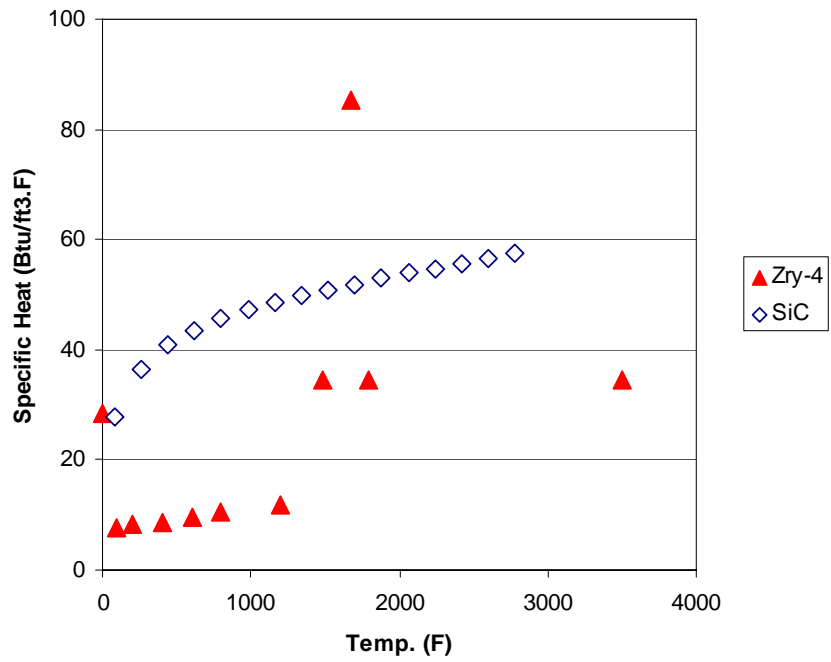


Figure 3-2 Specific Heat of Zry-4 and SiC

4. Fuel Rod Analysis

4.1 Methodology

A typical 17×17 PWR fuel rod is considered whose geometry is shown in Figure 4-1. The geometry is composed of fuel, gap, and cladding. The specific parameters are shown in Table 2-1. The purpose is to analyze cladding from the structural mechanical point of view.

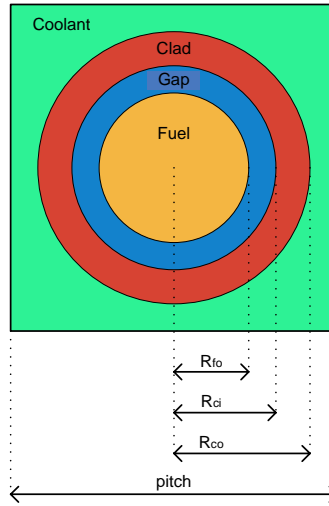


Figure 4-1 Schematic Cross-Section of a Fuel Cell

It is not appropriate to apply a thin shell model for the analysis since $t/R_{ci} > 0.1$. So a thick wall model is used to calculate the stress profile. The derivations are based on M. Kazimi^[5].

Force equilibrium in radial direction:

$$\frac{d\sigma_r}{dr} + \frac{\sigma_r - \sigma_\theta}{r} = 0 \quad \text{Eq-1}$$

Hook's law:

$$\varepsilon_r = \frac{1}{E} [\sigma_r - \nu(\sigma_\theta + \sigma_z)] \quad \text{Eq-2}$$

$$\varepsilon_\theta = \frac{1}{E} [\sigma_\theta - \nu(\sigma_r + \sigma_z)] \quad \text{Eq-3}$$

$$\varepsilon_z = \frac{1}{E} [\sigma_z - \nu(\sigma_\theta + \sigma_r)] \quad \text{Eq-4}$$

Strain-displacement relationships:

$$\varepsilon_\theta = u / r \quad \text{Eq-5}$$

$$\varepsilon_r = du / dr \quad \text{Eq-6}$$

By manipulating Eq-5 and Eq-6, we get:

$$\frac{d\varepsilon_\theta}{dr} = \frac{1}{r}(\varepsilon_r - \varepsilon_\theta) \quad \text{Eq-7}$$

Since we are considering for a closed cylinder far from the end, σ_z is assumed to be constant. Applying Eq-2 and Eq-3 into Eq-5, we get:

$$\frac{d}{dr}(\sigma_r + \sigma_\theta) = 0 \quad \text{Eq-8}$$

Considering Eq-6 with Eq-1, we get

$$\frac{d}{dr} \frac{1}{r} \frac{d}{dr}(r^2 \sigma_r) = 0 \quad \text{Eq-9}$$

Boundary condition:

$$\sigma_r(r = R_{ci}) = -P_i \quad \text{Eq-10}$$

$$\sigma_r(r = R_{co}) = -P_o \quad \text{Eq-11}$$

Since the axial stress has less dependency on the radial direction compared to radial and hoop directional stresses, it is regarded as a constant along variable r. After solving Eq-8 and Eq-9 with Eq-10 and Eq-11, the solutions are:

$$\sigma_r = -P_i \left(\frac{R_{ci}}{r}\right)^2 + \left[1 - \left(\frac{R_{ci}}{r}\right)^2\right] \frac{-P_o R_{co}^2 + P_i R_{ci}^2}{R_{co}^2 - R_{ci}^2} \quad \text{Eq-12}$$

$$\sigma_\theta = P_i \left(\frac{R_{ci}}{r}\right)^2 + \left[1 + \left(\frac{R_{ci}}{r}\right)^2\right] \frac{-P_o R_{co}^2 + P_i R_{ci}^2}{R_{co}^2 - R_{ci}^2} \quad \text{Eq-13}$$

$$\sigma_z = \frac{\pi R_{ci}^2 P_i - \pi R_{co}^2 P_o}{\pi(R_{co}^2 - R_{ci}^2)} \quad \text{Eq-14}$$

When the Fourier conduction equation is solved under a cylindrical geometry with no internal heat generation, a temperature profile usually follows a logarithmic function. For the logarithmic temperature profile, thermal stress can be obtained from J. Harvey^[6].

$$\sigma_r^{th} = \frac{\alpha E \Delta T}{2(1-\nu) \ln\left(\frac{R_{co}}{R_{ci}}\right)} \left[-\ln\left(\frac{R_{co}}{r}\right) - \frac{R_{ci}^2}{R_{co}^2 - R_{ci}^2} \left(1 - \frac{R_{co}^2}{r^2}\right) \ln\left(\frac{R_{co}}{R_{ci}}\right) \right] \quad \text{Eq-15}$$

$$\sigma_\theta^{th} = \frac{\alpha E \Delta T}{2(1-\nu) \ln\left(\frac{R_{co}}{R_{ci}}\right)} \left[1 - \ln\left(\frac{R_{co}}{r}\right) - \frac{R_{ci}^2}{R_{co}^2 - R_{ci}^2} \left(1 + \frac{R_{co}^2}{r^2}\right) \ln\left(\frac{R_{co}}{R_{ci}}\right) \right] \quad \text{Eq-16}$$

$$\sigma_z^{th} = \frac{\alpha E \Delta T}{2(1-\nu) \ln\left(\frac{R_{co}}{R_{ci}}\right)} \left[1 - 2 \ln\left(\frac{R_{co}}{r}\right) - \frac{2R_{ci}^2}{R_{co}^2 - R_{ci}^2} \ln\left(\frac{R_{co}}{R_{ci}}\right) \right] \quad \text{Eq-17}$$

$$T_w(r) = T_{wo} + \Delta T \frac{\ln(R_{co}/r)}{\ln(R_{co}/R_{ci})} \quad \text{Eq-18}$$

, where α and ΔT are the thermal expansion coefficient and the temperature difference between inner wall and outer wall, respectively.

Since the primary stresses are defined as external stresses, the only primary stress for this analysis is due to the inner and outer cladding pressure difference. The secondary stresses are due to a constraint. For this analysis, only thermal stress is considered as the secondary stress. For the failure criteria ASME code are utilized.

ASME code:

$$P_m \leq S_m \leq \min\left(\frac{2}{3}\sigma_y, \frac{1}{3}\sigma_u\right) \quad \text{Eq-19}$$

$$P_m + Q \leq 3S_m \leq 3 \min\left(\frac{2}{3}\sigma_y, \frac{1}{3}\sigma_u\right) \quad \text{Eq-20}$$

, where P_m and Q are the primary and thermal stresses respectively.

Since $(\sigma_r, \sigma_\theta, \sigma_z)$ and $(\sigma_r', \sigma_\theta', \sigma_z')$ are the primary and secondary principal stresses, P_m and $P_m + Q$ can be calculated by TRESCA theory:

$$P_m = \max\left(|\sigma_r - \sigma_\theta|, |\sigma_\theta - \sigma_z|, |\sigma_z - \sigma_r|\right) \quad \text{Eq-21}$$

$$P_m + Q = \max\left(|\sigma_r' - \sigma_\theta'|, |\sigma_\theta' - \sigma_z'|, |\sigma_z' - \sigma_r'|\right) \quad \text{Eq-22}$$

$$\sigma_r' = \sigma_r + \sigma_r^{th} \quad \text{Eq-23}$$

$$\sigma_\theta' = \sigma_\theta + \sigma_\theta^{th} \quad \text{Eq-24}$$

$$\sigma_z' = \sigma_z + \sigma_z^{th} \quad \text{Eq-25}$$

4.2 Boundary Condition

A typical 4-loop Westinghouse PWR is selected as a reference plant. Three RELAP5 models were developed to get the boundary condition during steady-state and LBLOCA for different cladding materials. The steady state conditions, which are initial conditions for LBLOCA, were obtained through simulations as shown in Table 4-1.

Table 4-1 Steady-State Initialization

Parameters	Desired	Simulated
Core Power (MWth)	3479.2	3479.2
Pressurizer Pressure (bar)	155.1	155.1
Cold Leg Temp. (K)	564.85	566.61
Hot Leg Temp. (K)	599.25	598.71
Total Loop Flow (kg/s)	18630.0	18714.3
Effective Core Flow (kg/s)	17700.0	17857.2
Bypass Flow Fraction (%)	5.0	4.58
SG Secondary Pressure (bar)	58.0	61.8

The gap pressure is assumed to be constant during steady state and LBLOCA. Although three RELAP5 models are based on different cladding materials, all the thermal hydraulics properties given in Table 4-1 and Figure 4-2 are the same for each model since the operating conditions are the same for each cladding materials.

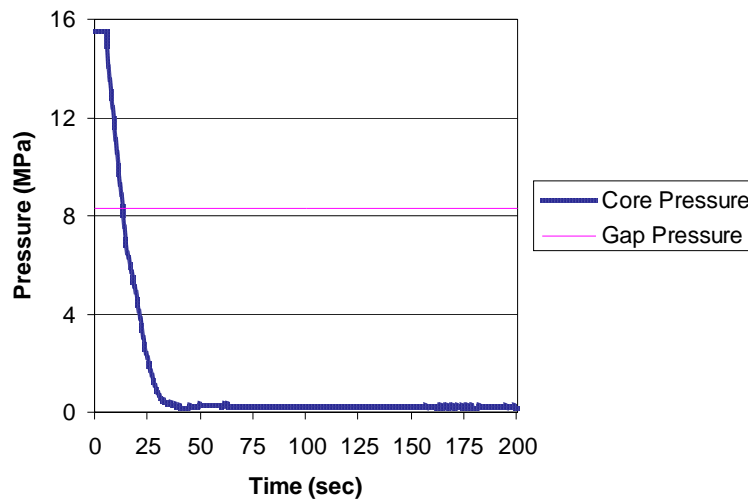


Figure 4-2 Pressure of Fuel Gap and Reactor Core during LBLOCA

Figures 4-3 and 4-4 show the cladding outer surface temperature of the hottest fuel pin. Figure 4-3 shows the maximum temperature during the blowdown and Figure 4-4 shows the maximum temperature during reflood period. Although the irradiated SiC cladding during reflood shows the highest cladding temperature, it still has a sufficient margin compared to the regulatory limit of 1473K which is more than 16.14% safety margin.

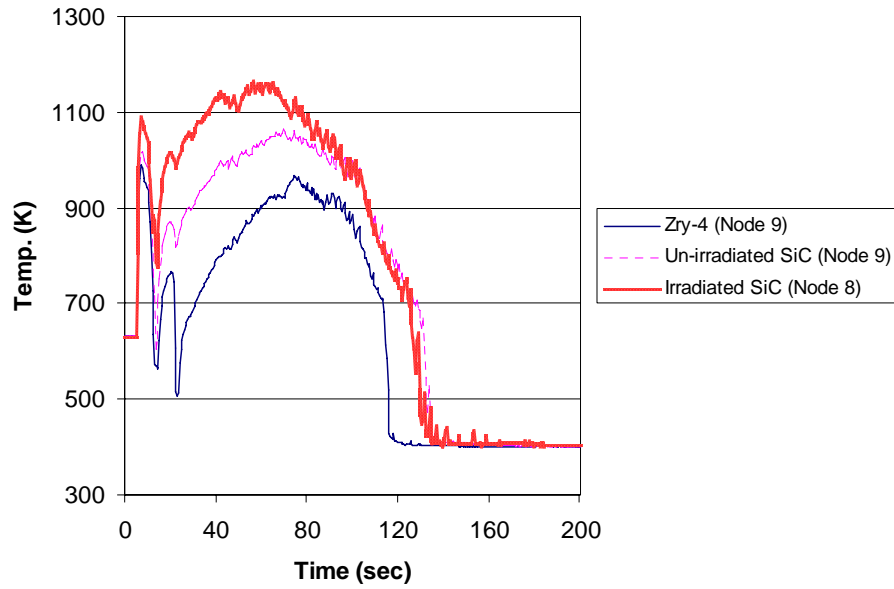


Figure 4-3 Outer Peak Clad Temp. during LBLOCA (Blowdown)

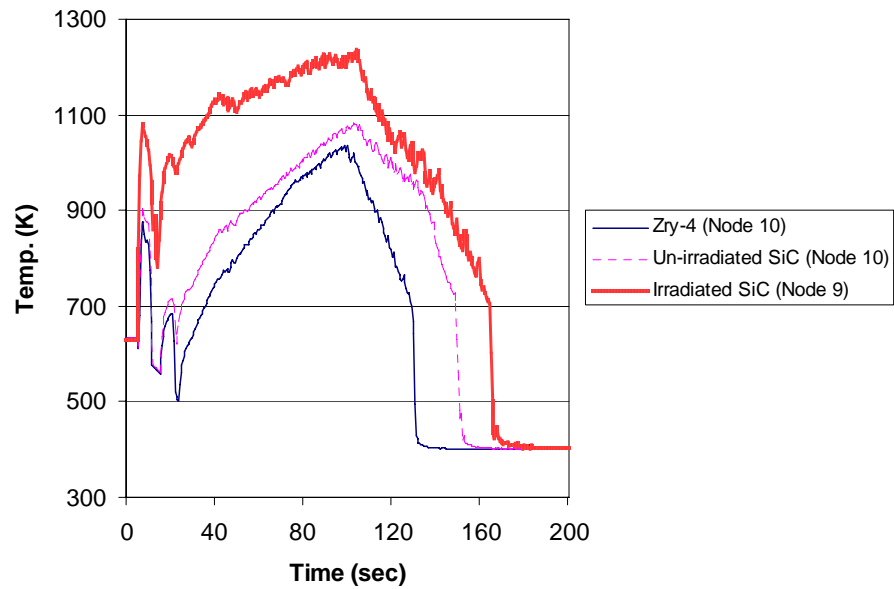


Figure 4-4 Outer Peak Clad Temp. during LBLOCA (Reflood)

Figures 4-5 and 4-6 show the cladding inner surface temperature of the hottest fuel pin. Figure 4-5 shows the maximum temperature during the blowdown and Figure 4-6 shows the maximum temperature during reflow period. Although the irradiated SiC cladding during reflow shows the highest cladding temperature, it still has a sufficient margin compared to the regulatory limit of 1473K which is more than a 15.68% safety margin.

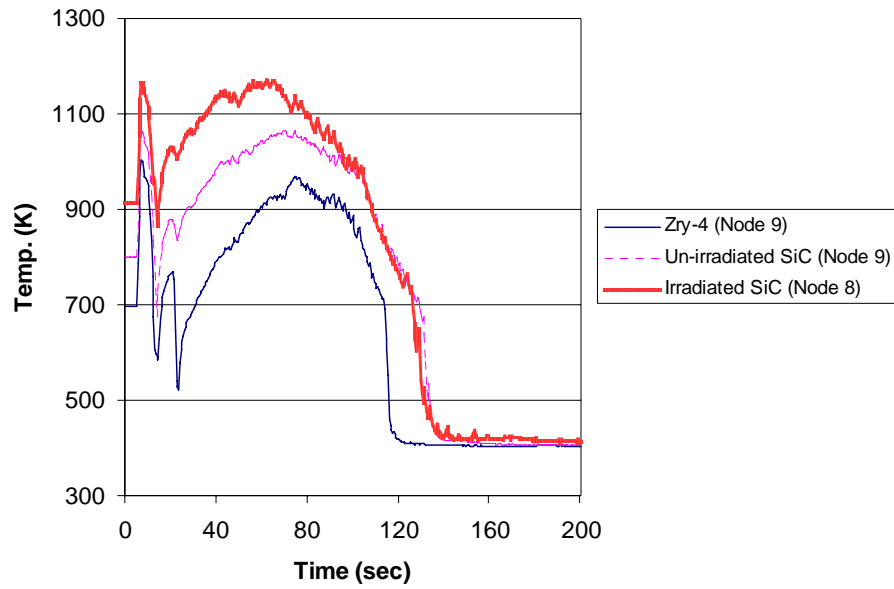


Figure 4-5 Inner Peak Clad Temp. during LBLOCA (Blowdown)

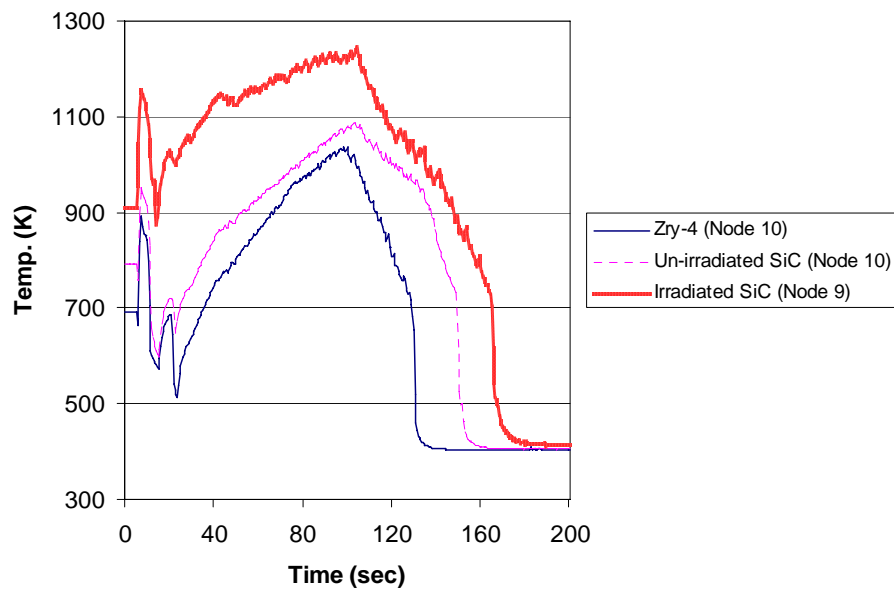


Figure 4-6 Inner Peak Clad Temp. during LBLOCA (Reflow)

4.3 Results

Since the primary and secondary stresses are stabilized before 40 seconds after LBLOCA, both stresses are analyzed during 40 seconds after LBLOCA. Next four figures show the primary stress distributions. All the primary stresses are the same for three materials due to the same inner and outer cladding pressure.

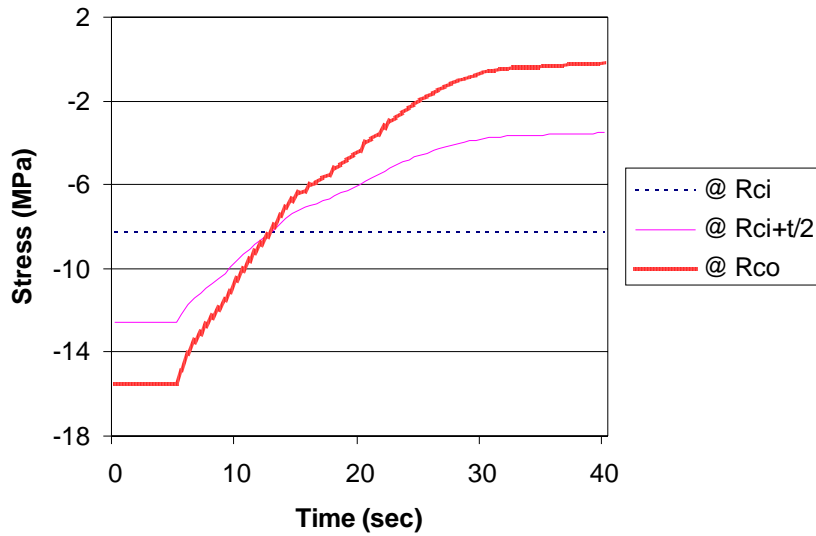


Figure 4-7 Pressure Induced Radial Stress Distribution

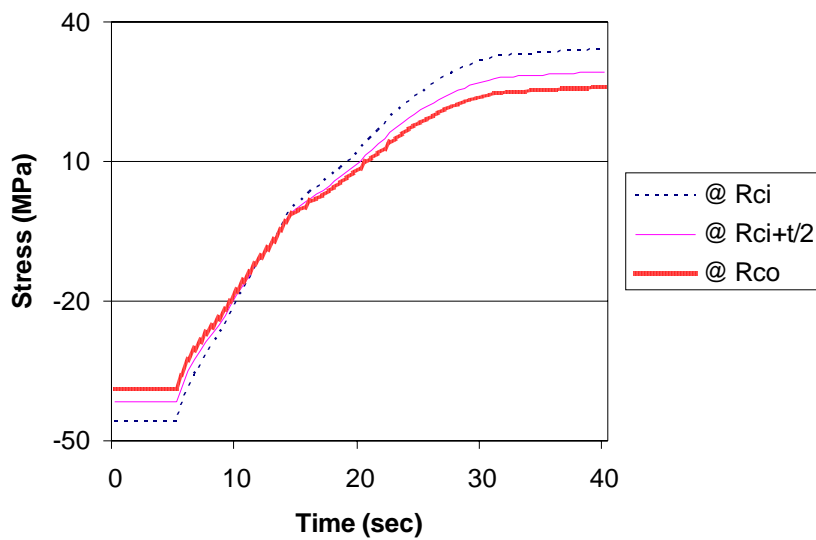


Figure 4-8 Pressure Induced Hoop Stress Distribution

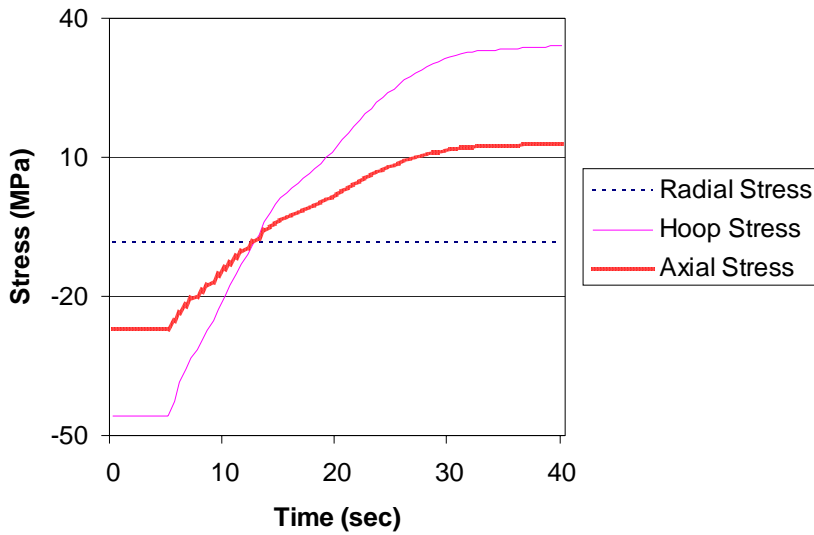


Figure 4-9 Pressure Induced Stress Distribution at Cladding Inner Surface

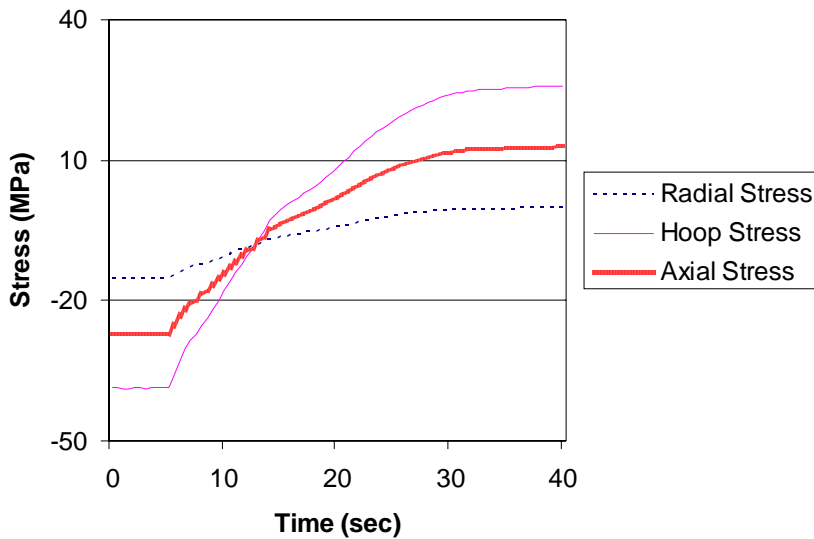


Figure 4-10 Pressure Induced Stress Distribution at Cladding Outer Surface

Next three figures show the secondary stress distributions which include the pressure induced stress and thermal stress distributions. Three cladding materials Zry-4, Un-irradiated SiC, and Irradiated SiC have the different inner and outer temperature profiles due to different thermal conductivities. It should be noted that three figures have different y-axis scales. Zry-4 has the least fluctuation of stress history and Irradiated SiC shows the largest fluctuation of stress history.

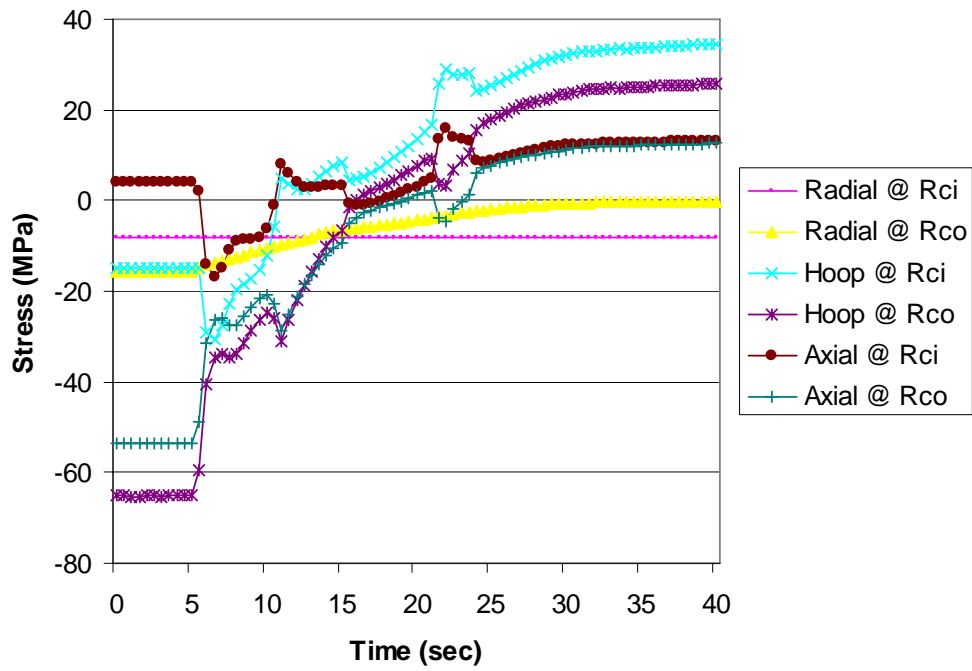


Figure 4-11 Secondary Stress Distribution for Zry-4 clad

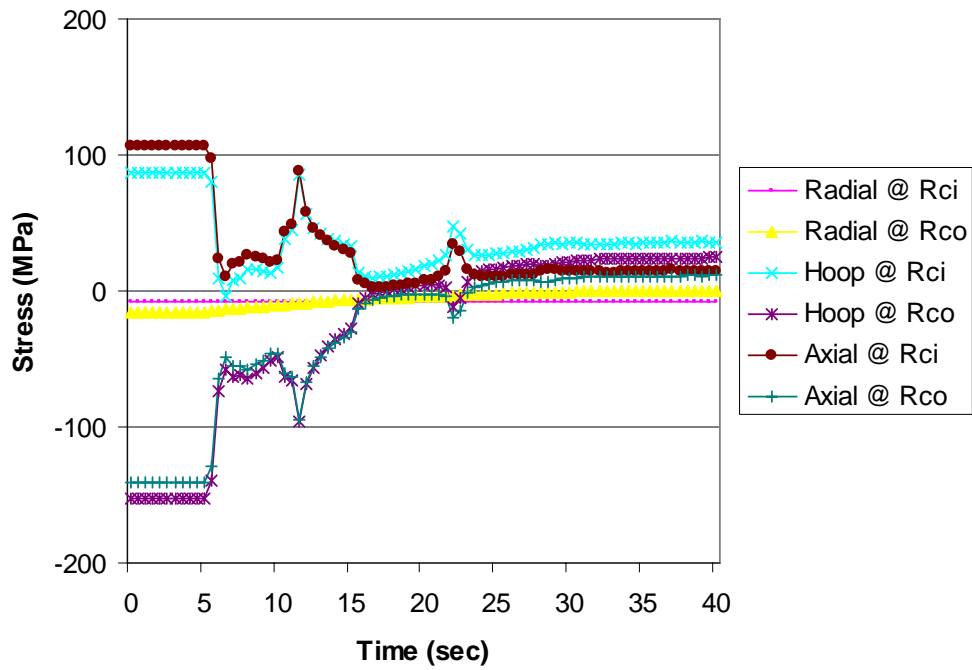


Figure 4-12 Secondary Stress Distribution for Un-irradiated SiC clad

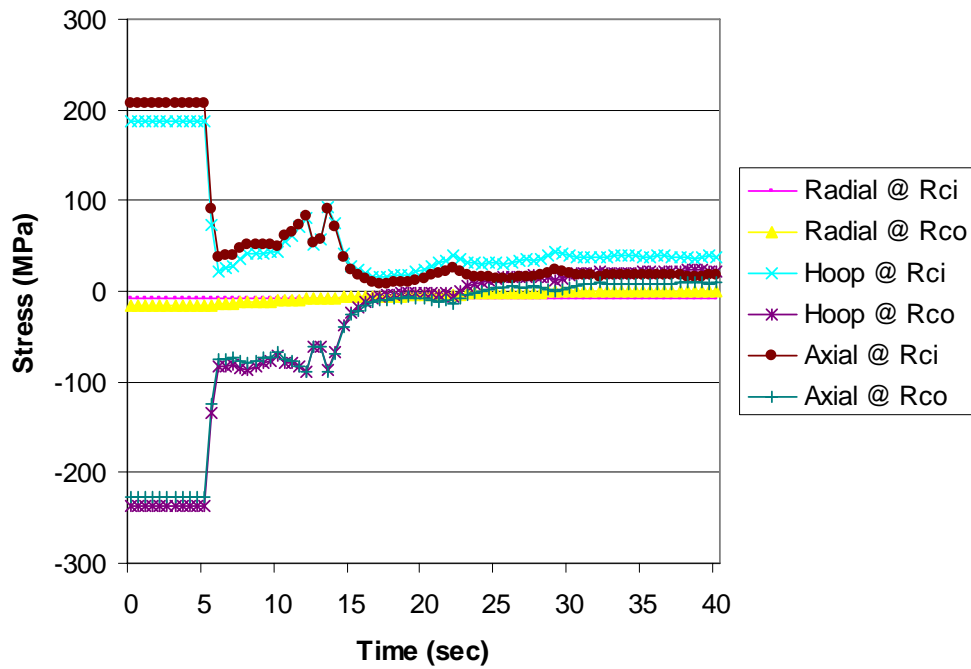


Figure 4-13 Secondary Stress Distribution for Irradiated SiC clad

Figure 4-14 shows the TRESCA stress history during LBLOCA at three different radial points: cladding inner surface, centerline, and outer surface. Figures 4-15 and 4-16 also show the TRESCA history during LBLOCA for all three cladding materials. Figure 4-15 shows the cladding stress at inner surface and Figure 4-16 shows the stress at outer surface.

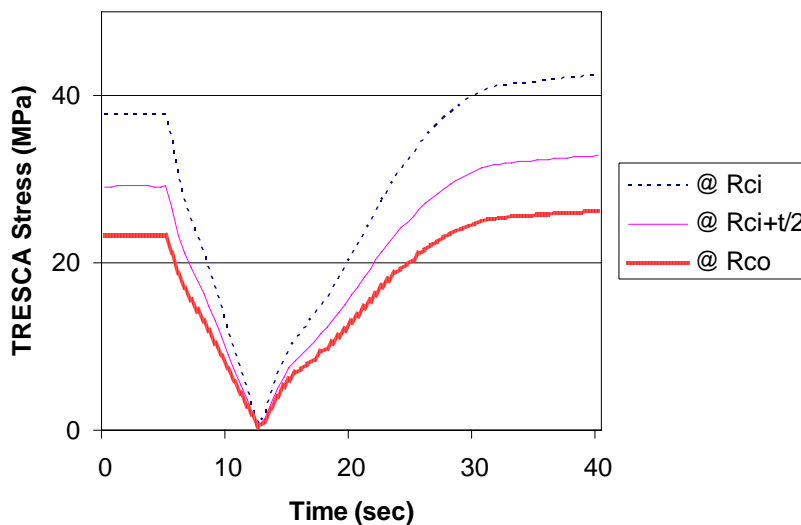


Figure 4-14 TRESCA Stress: Pressure Induced Only

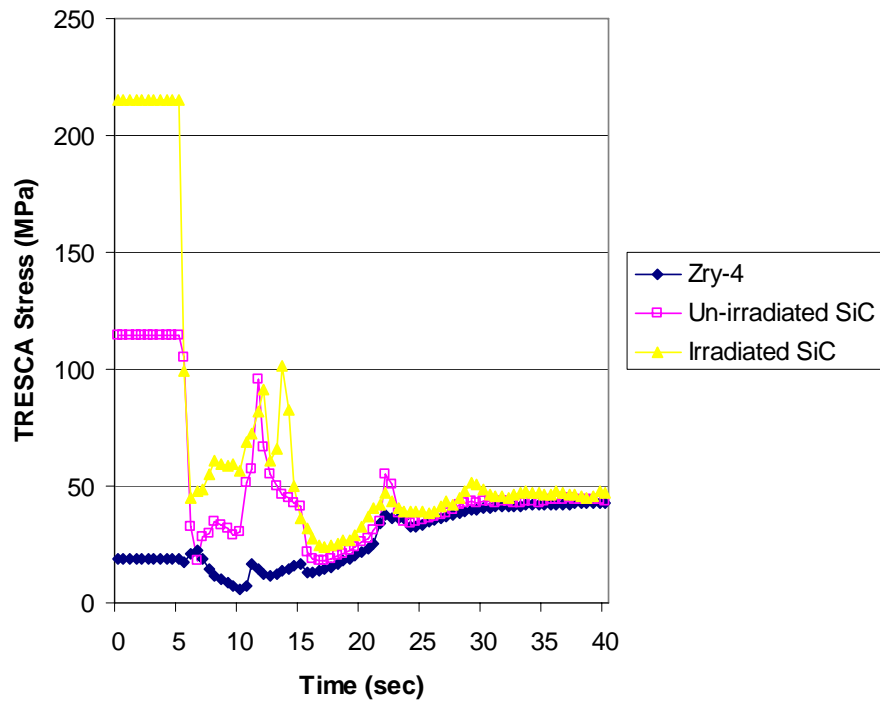


Figure 4-15 Secondary Tresca Stress at Cladding Inner Surface

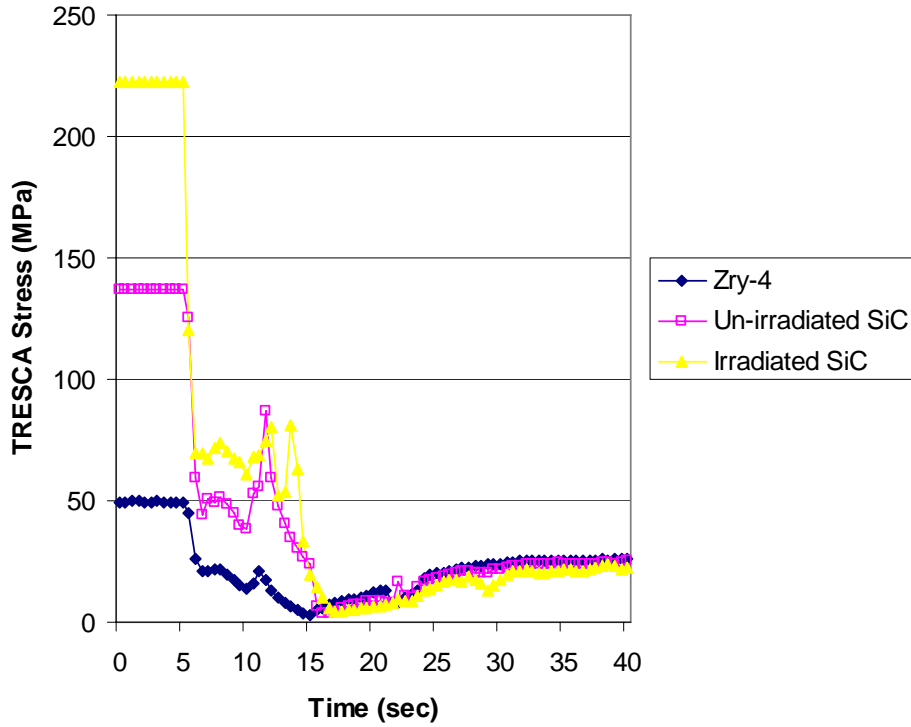


Figure 4-16 Secondary Tresca Stress at Cladding Outer Surface

From the figures, it is clearly seen that all the TRESCA stresses reach quasi steady-state value before 40 seconds after the initiation of LBLOCA. Since the temperature profiles change until 180 seconds, it is mainly due to the pressure induced stresses. The maximum TRESCA stress in all three figures is approximately at 4 seconds after the initiation of LBLOCA. It corresponds to the initial peak temperature in the reflood boundary condition.

If ASME code is applied for design, Figure 4-17 is in the primary category given by Eq-19, and Figure 4-18 and 4-19 are included in the secondary category given by Eq-20. Thus it can be concluded that in Figure 4-11 limiting material properties are:

$$P_m \leq S_m \leq \min\left(\frac{2}{3}\sigma_y, \frac{1}{3}\sigma_u\right) = \min\left(\frac{2}{3} \cdot 170, \frac{1}{3} \cdot 241\right) = 80.33 \text{ MPa} \quad \text{for Zry-4}$$

$$P_m \leq S_m \leq \min\left(\frac{2}{3}\sigma_y, \frac{1}{3}\sigma_u\right) = \min\left(\frac{2}{3} \cdot 450, \frac{1}{3} \cdot 450\right) = 150 \text{ MPa} \quad \text{for SiC}$$

The limiting material properties in Figure 4-12 and 4-13 are:

$$P_m + Q \leq 3S_m \leq \min(2\sigma_y, \sigma_u) = 3 \cdot (80.33) = 160.66 \text{ MPa} \quad \text{for Zry-4}$$

$$P_m + Q \leq 3S_m \leq \min(2\sigma_y, \sigma_u) = 3 \cdot (150) = 300 \text{ MPa} \quad \text{for SiC}$$

From Figure 4-14 to Figure 4-16 show the Safety Margin which corresponds to previous three figures. In Figure 4-14 SiC has more margin than Zry-4 at every time but in Figure 4-15 and 16 the safety margin fluctuate as time going on due to oscillating temperature profiles.

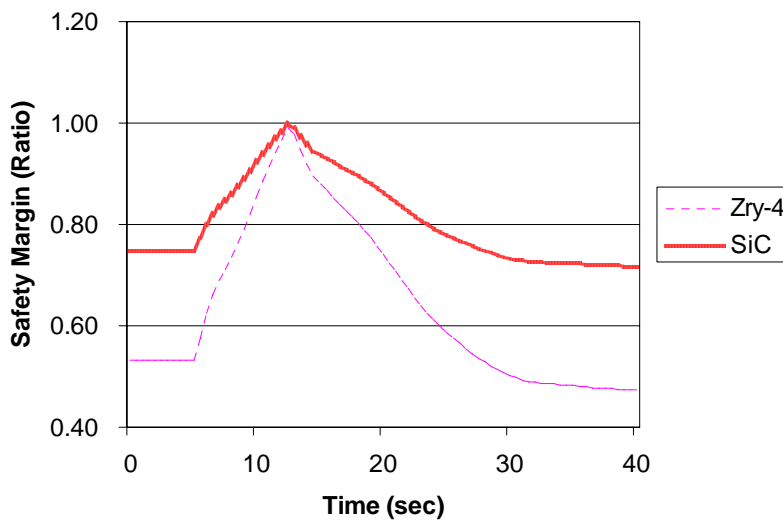


Figure 4-17 Safety Margin: Pressure Induced Only at Cladding Inner Surface

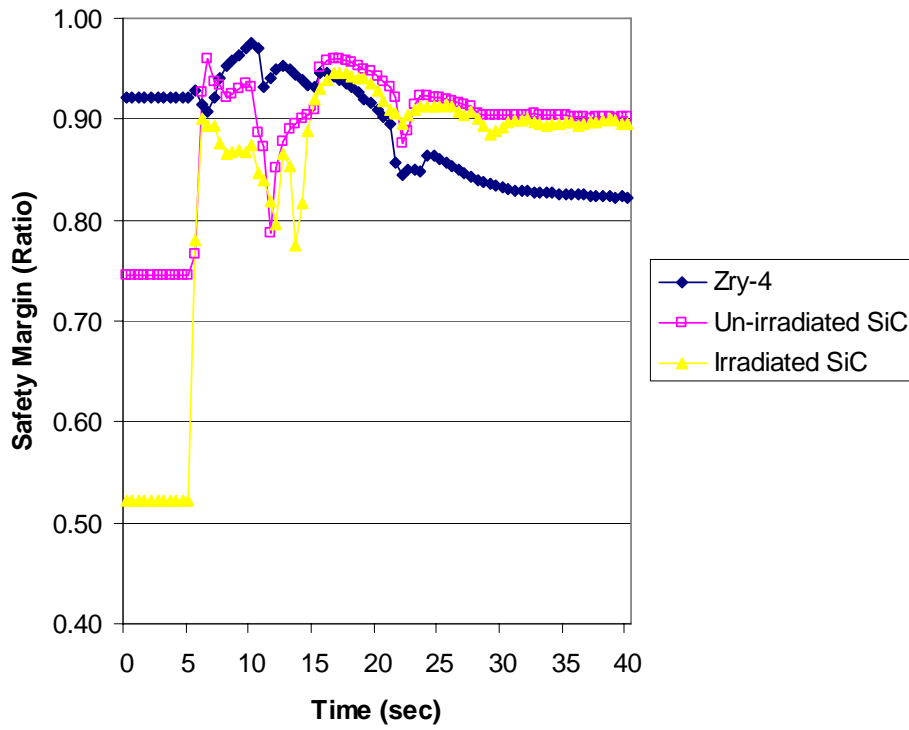


Figure 4-18 Secondary Stress Intensity Safety Margin at Cladding Inner Surface

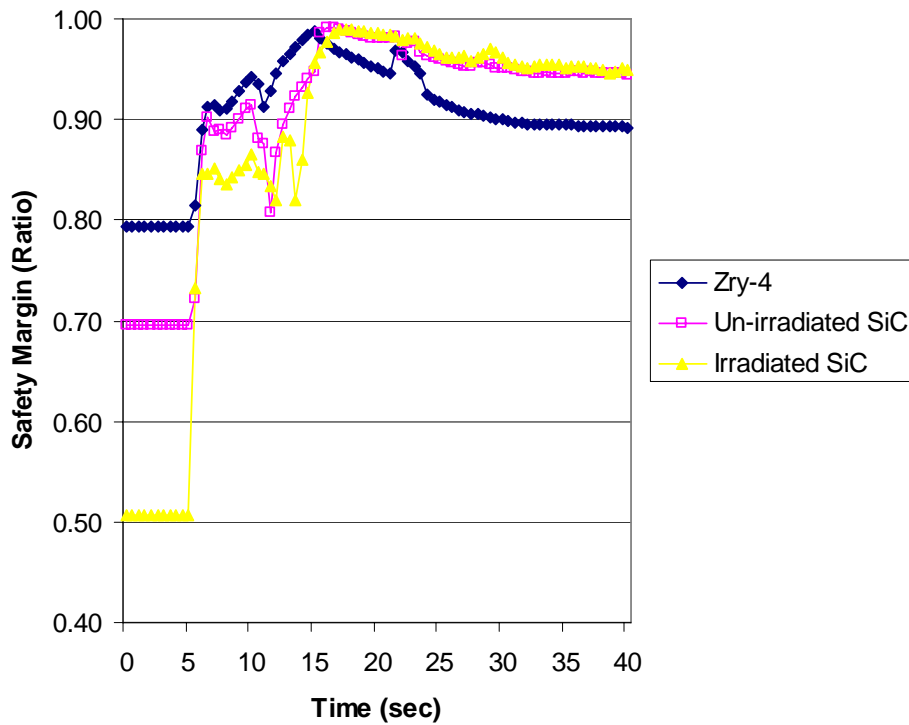


Figure 4-19 Secondary Stress Intensity Safety Margin at Cladding Outer Surface

5. Conclusion

The primary stresses of all three cladding materials: Zry-4, Un-irradiated SiC, and Irradiated SiC, are the same, as shown in Figures 4-7, 4-8, 4-9, and 4-10. This is because during LOCA transient the cladding outer pressure history is not affected by cladding materials. The cladding outer surface experiences larger radial stress changes than the inner surface, while the cladding inner surface experiences larger hoop stress changes than the outer surface. The hoop stress is one of the largest stresses and the radial stress is the smallest among all three directional stresses, when only the primary stresses are considered.

However, since the thermal stresses are considered for calculating the secondary stresses and the temperature histories in the cladding are all different for cladding materials, secondary stresses behave differently for all three materials. In all three materials the maximum stress is at the cladding outer surface. Zry-4 shows the smallest fluctuation with the smallest magnitude compared to others, and irradiated SiC shows the largest fluctuation with the largest one. Since cladding outer surface pressure converges to a single value before 40 seconds after the LBLOCA and the temperature oscillates until 180 seconds, the secondary stress is initially dominated by the thermal stress and after 40 seconds by the primary stress.

The primary stress intensity has a maximum at cladding inner surface and a minimum at outer surface. All the secondary stress intensities are stabilized around 30 seconds after the LBLOCA. The secondary stress intensity shows the same behavior with the primary TRESCA stress and the primary TRESCA value at the end of transient is approximately the same for all cases, since the primary stress dominates towards the end of the transient. In the beginning of LBLOCA, the stress applied to Zry-4 is the smallest while irradiated SiC is the largest, but all these materials finally converge to a similar value.

In terms of the primary stresses, the SiC has higher safety margin than Zry-4 due to higher yield and ultimate strengths with the same primary TRESCA stress. However, considering the secondary stresses, Zry-4 performs better than the two SiC cases before 5 seconds after the LBLOCA due to its high thermal conductivity which reduces the temperature gradient between the inner and outer surfaces of the cladding. After the 5 seconds, since the primary stresses dominate over the thermal stresses, the SiC cladding shows better performance in terms of the safety margin. The irradiated SiC always performs worse than the un-irradiated SiC, as the thermal conductivity of the irradiated one is lower than the un-irradiated one.

The Gap pressure is assumed constant. But as the burnup increases, the gap pressure will increase due to fission gas release. Young's modulus, yield strength, and ultimate strength are also considered constant but they depend on temperature. Moreover we did not consider the creep, strain, displacement, and junction discontinuity. Modeling and considering these kinds of input parameter more exactly, we can set up and get more realistic model and results. In the simulation cases, we can also investigate the power up-rate case and another transient analysis like LOFA, these cases can give us ideas about more broad understanding, pros and cons of SiC in Nuclear applications. And if we use well-developed simulation code for structural analysis codes like FRAPTRAN, we can make our future study in a realistic and easy manner.

Reference

- [1] D. Feng, M. S. Kazimi, and P. Hejzlar, "Innovative Fuel Designs for High Power Density Pressurized Water Reactor," MIT-NFC-TR-075, September 2005
- [2] D. M. Carpenter, "Assessment of Innovative Fuel Designs for High Performance Light Water Reactors," Master Thesis at MIT, June 2006
- [3] D. C. Larson, J. W. Adams, L. R. Johnson, A. P. S. Teotia, and H. G. Hill, "Ceramic Materials for Advanced Heat Engines - Technical and Economic Evaluation," Noyes Publications, 1984
- [4] N. E. Todreas and M. S. Kazimi, "Nuclear Systems: Vol.1," Francis and Taylor, 1990
- [5] M. S. Kazimi, "Lecture Notes and Problem Sets in Course 22.314," MIT, 2006
- [6] J. F. Harvey, "Pressure Vessel Design: Nuclear and Chemical Applications," D. Van Nostrand Company Inc., Princeton, New Jersey, 1963
- [7] W. Chang, "Technical Data Sheet - Reactor Grade Zirconium Alloys for Nuclear Waste Disposal," Allegheny Technologies, 2003
- [8] CoorsTek, "Amazing Solutions: Advanced Silicon Carbide for Critical Components," CoorsTek F0401 8510-1024, 2005
- [9] J. A. DiCarlo, "High-Performance SiC/SiC Ceramic Composite Systems Developed for 1315°C (2400°F) Engine Components," NASA/TM-2004-212729, 2004.
- [10] L. Tong and J. Weisman, "Thermal Analysis of Pressurized Water Reactors," American Nuclear Society, 1996